Transient Hydrogen Atom Adducts to Disulfides. Formation and Energetics

František Tureček,* Miroslav Polášek, Aaron J. Frank, and Martin Sadílek

Contribution from the Department of Chemistry, Bagley Hall, Box 351700, University of Washington, Seattle, Washington 98195-1700

Received October 22, 1999

Abstract: Hydrogen atom adducts to the disulfide bonds in dimethyl disulfide (**1**) and 1,2-dithiolan (**2**) were generated transiently by collisional electron transfer to gaseous cations $CH_3SS(H)CH_3^+$ (**1H**$^+$) and **2H**$^+$, respectively. Hypervalent radical **1H** dissociated completely on the 4.6 μs time scale to **1** + H$^\bullet$, CH_3SH + $CH_3S^\bullet$, and CH_3SSH + $CH_3^\bullet$. The sulfur-containing dissociation products were detected and identified by neutralization−reionization mass spectrometry. Radical **1H** was found to be weakly bound; the S−S, S−C, and S−H 0 K bond dissociation energies were calculated by a modified G2++(MP2) method as 8, 52, and 96 kJ mol^{-1}, respectively. The energy to drive these dissociations was supplied by Franck−Condon effects on vertical neutralization of **1H**$^+$ (161−230 kJ mol^{-1}). Two stereochemically distinct pathways were found for the exothermic hydrogen atom addition to **1**. A rear attack at the disulfide bond had a small activation energy, E_a = 9 kJ mol^{-1}, while a side attack had E_a = 33 kJ mol^{-1}. Collisional neutralization of **2H**$^+$ provided a fraction of nondissociating **2H** at equilibrium with open-ring isomers, $HS-CH_2CH_2CH_2-S^\bullet$ (*syn*-**5** and *anti*-**5**) and $HSS-CH_2CH_2CH_2^\bullet$ (*syn*-**6** and *anti*-**6**). Hydrogen atom addition to the disulfide bond in **2** was calculated to be 118 kJ mol^{-1} exothermic and proceeded via a rear attack mechanism without an energy barrier. Stereoelectronic effects in hydrogen atom capture by disulfide bonds are discussed.

Introduction

Additions of small radicals, such as hydrogen and halogen atoms, OH$^\bullet$, alkyl, etc., to unsaturated and aromatic molecules have been studied extensively,[1] whereas additions to saturated molecules (alcohols, ethers, amines, sulfides, selenides, etc.) have received less attention until recently.[2] Reaction of a hydrogen atom with a heteroatom in a saturated molecule can be viewed as forming a transient hypervalent radical[2a] that is usually too unstable to be detected in the condensed phase. Hypervalent radicals have been considered as elusive intermediates of reactions as diverse as radical substitution,[2] electrochemical reduction,[3,4] and dissociative recombination.[5,6]

Recently, electron attachment to multiply charged peptide and protein ions in the gas phase was studied by ion cyclotron resonance mass spectrometry,[7] and mechanisms were postulated that invoked intramolecular hydrogen atom transfer to disulfide bonds[8] (Scheme 1). The postulated hypervalent thiasulfonium radical dissociated by cleavage of the disulfide bond, leading to novel gas-phase fragmentations (electron capture dissociation, ECD)[7] that were useful for structure elucidation of peptide ions by mass spectrometry.[8] The hydrogen atom capture mechanism was supported by density functional theory calculations of a dimethyl disulfide−hydrogen atom adduct that indicated that H atom addition was exothermic.[8] However, these previous calculations used a small basis set and did not consider activation energies in the hydrogen atom addition step. The putative intermediates of H atom capture by the disulfide bonds could not be identified by mass spectrometry, and other possible

Scheme 1

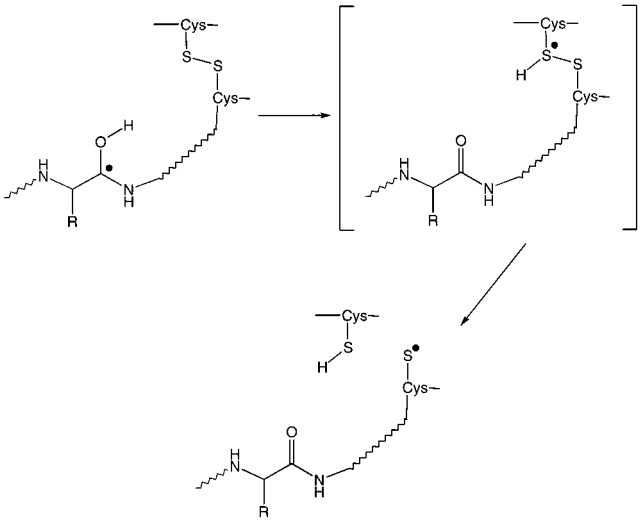

(1) For a review, see: Atkinson, R. *Gas-phase tropospheric chemistry of organic compounds*; Journal of Physical and Chemical Reference Data, Monograph 2; American Institute of Physics: Woodbury, NY, 1994.

(2) (a) Perkins, C. W.; Martin, J. C.; Arduengo, A. J.; Lau, W.; Alegria, A.; Kochi, J. K. *J. Am. Chem. Soc.* **1980**, *102*, 7753. (b) Smart, B. A.; Schiesser, C. H. *J. Comput. Chem.* **1995**, *16*, 1055. For a review, see: (c) Schiesser, C. H.; Wild, L. M. *Tetrahedron* **1996**, *52*, 13265.

(3) Gedye, R. N.; Sadana, Y. N. *J. Org. Chem.* **1980**, *45*, 3721.

(4) Kariv-Miller, E.; Nanjudiah, C.; Eaton, J.; Swenson, K. E. *J. Electroanal. Chem.* **1984**, *167*, 141.

(5) Bates, D. R. In *Dissociative Recombination*; Rowe, B. R., Mitchell, J. B. A., Canosa, A., Eds; NATO ASI Series; Plenum: New York, 1993; pp 1−10.

(6) Adams, N. G. In *Dissociative Recombination*; Rowe, B. R., Mitchell, J. B. A., Canosa, A., Eds; NATO ASI Series; Plenum: New York, 1993; pp 99−112.

(7) Zubarev, R. A.; Kelleher, N. L.; McLafferty, F. W. *J. Am. Chem. Soc.* **1998**, *120*, 3265.

(8) Zubarev, R. A.; Kruger, N. A.; Fridriksson, E. K.; Lewis, M. A.; Horn, D. M.; Carpenter, B. K.; McLafferty, F. W. *J. Am. Chem. Soc.* **1999**, *121*, 2857.

10.1021/ja993789q CCC: $19.00
Published on Web 02/24/2000

Scheme 2

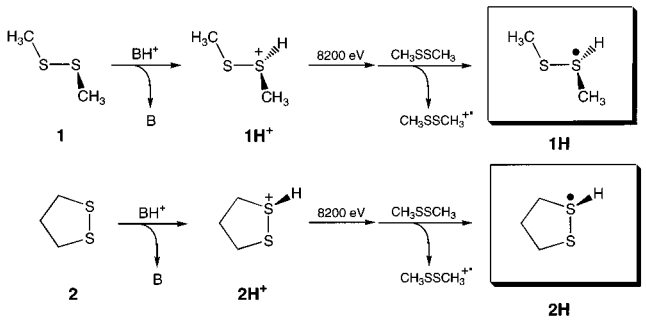

dissociation products resulting from bond cleavages in the vicinity of the hypervalent sulfur atom were difficult to distinguish in the mass spectra of multiply charged peptides.

Intramolecular hydrogen transfer from a hypervalent oxonium group, $R-O^{\bullet}(H)CH_3$, to a double bond had been observed previously and documented by deuterium labeling.[9] In contrast, hypervalent radicals with $R-NH_3^{\bullet}$ and $R-NH(CH_3)_2^{\bullet}$ groups were found not to transfer hydrogen atoms to a sterically accessible double bond, which was interpreted by energy barriers to both N−H bond dissociation and H atom addition to the double bond.[10] Additions of hydrogen atoms to sulfur atoms in hydrogen sulfide and dimethyl sulfide were found to be accompanied by substantial activation barriers.[2b,11,12] In contrast, radical centers in distonic ions have been shown to react with dimethyl disulfide in the gas phase by transfer of a methylthio group that involved cleavage of the S−S bond.[13] These previous findings rendered the postulated mechanism for H atom capture by the disulfide bond[8] very intriguing and motivated the present study.

While the formation of transient intermediates of hydrogen atom additions to saturated organic molecules is difficult to study in the condensed phase, such intermediates can be generated readily by collisional electron transfer to a stable gas-phase cation (Scheme 2). The cation is formed first by protonation with a gas-phase acid; the exothermicity of the protonation determines the internal energy of the cation.[14] Electron transfer from a polarizable thermal molecular donor (dimethyl disulfide, trimethylamine) to the cation that has been accelerated to a $>100\ 000\ m\ s^{-1}$ velocity lasts a few femtoseconds and produces the nascent radical with the structure and geometry of the precursor ion. This provides a nonchemical approach to hypervalent radicals that are detected on the time scale of a few microseconds by mass spectrometry following collisional ionization. This technique of neutralization−reionization mass spectrometry (NRMS)[15] has been used to generate and study a number of organic hypervalent onium radicals.[16]

We now use NRMS to generate and investigate hypervalent radicals having thiasulfonium groups that correspond to hydrogen atom adducts to disulfides. Dimethyl disulfide (**1**) is used as a model of a disulfide with a staggered conformation about the S−S bond.[17] As a model system with an eclipsed S−S bond we used 1,2-dithiolan (**2**), in which internal rotation is restricted by the five-membered ring. We will show by experiment that hypervalent thiasulfonium radicals undergo unimolecular cleavages of several bonds about the hypervalent sulfur atom. In addition, it will be shown by high-level ab initio and density functional theory calculations that hydrogen atom addition to the disulfide bond proceeds under stereoelectronic control that has substantial effects on the reaction rates.

Experimental Section

Methods. NRMS measurements were performed on a tandem quadrupole acceleration−deceleration mass spectrometer described previously.[18] Cation radicals $\mathbf{1}^{+\bullet}$, $\mathbf{2}^{+\bullet}$, and $CH_3SH^{+\bullet}$ were generated by electron ionization of the respective neutral molecules at 70 eV. Even-electron ions $\mathbf{1H}^+$and $\mathbf{2H}^+$ were prepared by gas-phase protonation with $CH_3C{=}NH^+/CH_3CN$ and $t\text{-}C_4H_9^+/2$-methylpropane, respectively, under conditions of chemical ionization (CI)[19] at 0.1−0.2 Torr of the reagent gas and 200−250 °C. $\mathbf{1D}^+$and $\mathbf{2D}^+$ were prepared by deuteronation with $CD_3C{=}ND^+/CD_3CN$ and/or $CD_3OD_2^+/CD_3OD$. The CI conditions were optimized to achieve efficient formation of $\mathbf{1H}^+-\mathbf{2D}^+$ and suppress the formation of $\mathbf{1}^{+\bullet}$, $\mathbf{2}^{+\bullet}$ in order to minimize contamination of the former ions by isobaric overlaps with ^{13}C, ^{33}S, and ^{34}S isotopomers of the latter.[11,12] Stable ions of 30−40 μs lifetimes were accelerated to 8250 eV and neutralized by collisions with dimethyl disulfide which was admitted at pressures to achieve 70% transmittance of the precursor ion beam. This corresponded mostly (>83%) to single-collision conditions. Remaining precursor ions were reflected electrostatically, and the neutral products were reionized by collisions with oxygen which was admitted at pressures to achieve 70% transmittance of the precursor ion beam. The flight times of the neutral intermediates were 4.6−4.9 μs for $\mathbf{1}^{+\bullet}-\mathbf{2D}^+$. The reionized ions were decelerated to 80 eV kinetic energy, energy-filtered, and mass-analyzed to provide NR mass spectra at unit mass resolution. Collisional activation of neutral intermediates was performed with helium which was admitted to achieve 50% and 70% transmittance of the precursor ion beam.[20]

Metastable ion and collisionally activated dissociations (CAD) of 10 keV ions were performed in the first field-free region of a JEOL HX-110 double-focusing mass spectrometer. Air was used as a collision

(9) Shaffer, S. A.; Sadilek, M.; Turecek, F.; Hop, C. E. C. A. *Int. J. Mass Spectrom. Ion Processes* **1997**, *160*, 137.
(10) Shaffer, S. A.; Wolken, J. K.; Turecek, F. *J. Am. Soc. Mass Spectrom.* **1997**, *8*, 1111.
(11) Sadilek, M.; Turecek, F. *Int. J. Mass Spectrom.* **1999**, *185/186/187*, 639.
(12) Sadilek, M.; Turecek, F. *J. Phys. Chem.* **1996**, *100*, 15027.
(13) Stirk, K. M.; Kiminkinen, L. K. M.; Kenttamaa, H. I. *Chem. Rev.* **1992**, *92*, 1649.
(14) (a) Nguyen, V. Q.; Turecek, F. *J. Am. Chem. Soc.* **1997**, *119*, 2280. (b) Nguyen, V. Q.; Turecek, F. *J. Mass Spectrom.* **1997**, *32*, 55.
(15) For reviews, see: (a) Wesdemiotis, C.; McLafferty, F. W. *Chem. Rev.* **1987**, *87*, 485. (b) Terlouw, J. K.; Schwarz, H. *Angew. Chem., Int. Ed. Engl.* **1987**, *26*, 805. (c) Holmes, J. L. *Mass Spectrom. Rev.* **1989**, *8*, 513. (d) Terlouw, J. K. *Adv. Mass Spectrom.* **1989**, *11*, 984. (e) McLafferty, F. W. *Science* **1990**, *247*, 925. (f) Turecek, F. *Org. Mass Spectrom.* **1992**, *27*, 1087. (g) Goldberg, N.; Schwarz, H. *Acc. Chem. Res.* **1994**, *27*, 347. (h) Schalley, C. A.; Hornung, G.; Schroder, D.; Schwarz, H. *Chem. Soc. Rev.* **1998**, *27*, 91. (i) Turecek, F. *J. Mass Spectrom.* **1998**, *33*, 779.
(16) (a) Wiliams, B. W.; Porter, R. F. *J. Chem. Phys.* **1980**, *73*, 5598. (b) Jeon, S.-J.; Raksit, A. B.; Gellene, G. I.; Porter, R. F. *J. Am. Chem. Soc.* **1985**, *107*, 4129. (c) Wesdemiotis, C.; Feng, R.; McLafferty, F. W. *J. Am. Chem. Soc.* **1986**, *108*, 5656. (d) Raksit, A. B.; Porter, R. F. *J. Chem. Soc., Chem. Commun.* **1987**, 500. (e) Selgren, S. F.; Gellene, G. I. *J. Phys. Chem.* **1987**, *87*, 5804. (f) Holmes, J. L.; Sirois, M. *Org. Mass Spectrom.* **1990**, *25*, 481. (g) Wesdemiotis, C.; Fura, A.; McLafferty, F. W. *J. Am. Soc. Mass Spectrom.* **1991**, *2*, 459. (h) Gu, M.; Turecek, F. *J. Am. Chem. Soc.* **1992**, *114*, 7146. (i) Sirois, M.; George, M.; Holmes, J. L. *Org. Mass Spectrom.* **1994**, *29*, 11. (j) Shaffer, S. A.; Turecek, F. *J. Am. Chem. Soc.* **1994**, *116*, 8647. (k) Shaffer, S. A.; Turecek, F. *J. Am. Soc. Mass Spectrom.* **1995**, *6*, 1004. (l) Shaffer, S. A.; Sadílek, M.; Turecek, F. *J. Org. Chem.* **1996**, *61*, 5234. (m) Sadilek, M.; Turecek, F. *J. Phys. Chem.* **1996**, *100*, 9610. (n) Nguyen, V. Q.; Sadilek, M.; Frank, A. J.; Ferrier, J. G.; Turecek, F. *J. Phys. Chem. A* **1997**, *101*, 3789. (o) Wolken, J. K.; Nguyen, V. Q.; Turecek, F. *J. Mass Spectrom.* **1997**, *32*, 1162. (p) Frøsig, L.; Turecek, F. *J. Am. Soc. Mass Spectrom.* **1998**, *9*, 242.
(17) (a) Beagley, B.; McAloon, K. T. *Trans. Faraday Soc.* **1971**, *67*, 3216. (b) Yokozeki, A.; Bauer, S. H. *J. Phys. Chem.* **1974**, *80*, 618. (c) Kuhler, M.; Charpentier, L.; Sutter, D.; Dreizler, H. *Z. Naturforsch., A: Phys., Phys. Chem., Kosmophys.* **1974**, *29A*, 1335.
(18) Turecek, F.; Gu, M.; Shaffer, S. A. *J. Am. Soc. Mass Spectrom.* **1992**, *3*, 493.
(19) Vairamani, M.; Mirza, U. A.; Srinivas, R. *Mass Spectrom. Rev.* **1990**, *9*, 235.
(20) (a) Danis, P.; Feng, R.; McLafferty, F. W. *Anal. Chem.* **1986**, *58*, 348. (b) Turecek, F.; Drinkwater, D. E.; Maquestiau, A.; McLafferty, F. W. *Org. Mass Spectrom.* **1989**, *24*, 669. (c) Shaffer, S. A.; Turecek, F.; Cerny, R. L. *J. Am. Chem. Soc.* **1993**, *115*, 12117.

gas at 70% and 50% precursor ion transmittance, and the spectra were obtained by an E/B linked scan at >500 mass resolution.

Materials. Dimethyl disulfide was purchased from Aldrich and used as received. 1,2-Dithiolan (**2**) was prepared by oxidation of 1,3-propanedithiol (Aldrich) with 30% hydrogen peroxide in acetic acid.[21] Monomeric **2** was distilled from the polymeric material directly into the vacuum system of the mass spectrometer and characterized by the electron ionization mass spectrum.[22] CD_3CN and CD_3OD (both Cambridge Isotope, 99% D) were used as received.

Calculations. Standard ab initio calculations were performed by using the Gaussian 98 suite of programs.[23] Geometries were optimized with density functional theory calculations using Becke's hybrid B3LYP functional[24] and the 6-31+G(2d,p) basis set. The optimized structures were characterized by harmonic frequency analysis as local minima (all frequencies real) and first-order saddle points (single imaginary frequency) and reoptimized at a uniform level with B3LYP/6-31++G(2d,p). For selected species, geometries were also optimized with Møller−Plesset theory calculations[25] truncated at second order, MP2(FULL) or MP2(frozen core)/6-31++G(2d,p), as discussed below. Transition state frequencies for H atom addition to **1** were obtained at the MP2(frozen core)/6-31+G(d,p) level of theory. Selected optimized geometries are presented in Figures 1, 2, 8, and 9. Spin-unrestricted calculations (UB3LYP and UMP2) were performed for open-shell species. Spin contamination in UMP2 calculations was small to moderate for most species; it was partially corrected by Schlegel's annihilation procedure[26] that decreased the total energies by 2−2.7 millihartree (2.3 millihartree rmsd). Atomic charges and spin populations were obtained by Mulliken population analysis of the UHF/6-31++G(2d,p) wave functions. The B3LYP frequencies were corrected by 0.963,[27] while the MP2 frequencies were corrected by 0.931 and used to calculate zero-point vibrational corrections. Thermal corrections were calculated using the rigid rotor−harmonic oscillator approximation. Complete optimized geometries (Cartesian coordinates), uncorrected harmonic frequencies, and total energies for all species are available as Supporting Information. Single-point energies were calculated at several levels of theory. The composite G2(MP2) procedure[28] was used to provide reference energies for ions derived from **1**. For hypervalent radicals, reaction products, and transition states derived from **1**, a slightly modified composite procedure was adopted that consisted of single-point QCISD(T)/6-31++G(d,p), PMP2/6-31++G(d,p), and PMP2/6-311++G(3df,2p) calculations that were combined according to eq 1.

$$\text{QCISD(T)/6-311++G(3df,2p)} \approx \text{QCISD(T)/6-31++G(d,p)} + \text{PMP2/6-311++G(3df,2p)} - \text{PMP2/6-31++G(d,p)} \quad (1)$$

Energies calculated at this effective level of theory and corrected for B3LYP/6-31+G(2d,p) zero-point vibrational energies are denoted as G2++(PMP2) by analogy with the G2(MP2) method, although they do not contain an empirical energy corrections for the number of valence electrons. The G2++(MP2) relative energies were within 1.7 kJ mol^{-1} rmsd of G2(PMP2) energies for five test systems out of the current set involving cations, molecules, and radicals. Comparison with experimental data was made for the S−S and S−C bond dissociation energies in **1** that were reproduced within the experimental uncertainties (Table 3). In addition, B3LYP single-point energies were calculated with the 6-311++G(3df,2p) and aug-cc-pVTZ basis sets. Using the much larger aug-cc-pVTZ basis set[29] did not provide any significant improvement in the B3LYP calculated relative energies. The B3LYP/6-311++G(3df,2p) single-point energies were averaged with the PMP2/6-311++G(3df,2p) energies available from the G2++(MP2) calculations. We showed previously[30] that empirical averaging of PMP2 and B3LYP relative energies obtained with adequately large basis sets provided improved fit with experimental data or results from high-level calculations. For 15 relative energies calculated for dimethyl disulfide-related cations, molecules, and radicals, the averaged B3LYP and PMP2 energies were within 8.4 kJ mol^{-1} rmsd of the G2++(PMP2) data. The rmsd's for the PMP2 and B3LYP relative energies were 11.7 and 16.1 kJ mol^{-1} relative to G2++(PMP2). Thus, averaging the B3LYP and PMP2 data resulted in a substantially improved relative energies because of cancellation of errors inherent to these two methods.[15i]

For ion and radical systems derived from **2**, higher level QCISD(T) calculations required scratch files in excess of 6 GB and were beyond our computational capabilities. Therefore, single-point energies were calculated with B3LYP and PMP2 using the 6-311++G(2df,p) basis set, and the relative energies were averaged.

Thermal rate constants were calculated using standard transition state theory formulas.[31] The activation energies were from G2++(PMP2) or averaged B3LYP and PMP2 calculations. Partition functions were calculated from B3LYP/6-31+G(2d,p) moments of inertia and corrected harmonic frequencies. Franck−Condon effects in vertical neutralization and ionization were taken as absolute differences between the total energies of fully optimized ion or neutral structures and those in which an electron has been added to an optimized ion structure or subtracted from an optimized neutral structure. No zero-point corrections were used in the calculated Franck−Condon energies.

Results and Discussion

Protonation of Dimethyl Disulfide. Successful generation of transient neutral species by NRMS necessitates unambiguous preparation and characterization of the pertinent precursor ions. Those for (**1** + H) adducts were generated by gas-phase protonation of **1** with $CH_3C{=}NH^+$ (eq 2); the latter reagent was formed by chemical self-ionization of acetonitrile.[19] Gas-phase deuteronation was performed analogously using $CD_3C{=}ND^+$ (eq 3).

$$CH_3SSCH_3 + CH_3C{=}NH^+ \rightarrow \mathbf{1H}^+ + CH_3CN \quad (2)$$

$$CH_3SSCH_3 + CD_3C{=}ND^+ \rightarrow \mathbf{1D}^+ + CD_3CN \quad (3)$$

According to the tabulated proton affinities (PA)[32] of **1** (PA =

(21) Field, L.; Barbee, R. B. *J. Org. Chem.* **1969**, *34*, 36.
(22) NIST/EPA/NIH Mass Spectral Library; http://webbook.nist.gov/chemistry.
(23) Frisch, M. J.; Trucks, G. W.; Schlegel, H. B.; Scuseria, G. E.; Robb, M. A.; Cheeseman, J. R.; Zakrzewski, V. G.; Montgomery, J. A., Jr.; Stratmann, R. E.; Burant, J. C.; Dapprich, S.; Millam, J. M.; Daniels, A. D.; Kudin, K. N.; Strain, M. C.; Farkas, O.; Tomasi, J.; Barone, V.; Cossi, M.; Cammi, R.; Mennucci, B.; Pomelli, C.; Adamo, C.; Clifford, S.; Ochterski, J.; Petersson, G. A.; Ayala, P. Y.; Cui, Q.; Morokuma, K.; Malick, D. K.; Rabuck, A. D.; Raghavachari, K.; Foresman, J. B.; Cioslowski, J.; Ortiz, J. V.; Stefanov, B. B.; Liu, G.; Liashenko, A.; Piskorz, P.; Komaromi, I.; Gomperts, R.; Martin, R. L.; Fox, D. J.; Keith, T.; Al-Laham, M. A.; Peng, C. Y.; Nanayakkara, A.; Gonzalez, C.; Challacombe, M.; Gill, P. M. W.; Johnson, B.; Chen, W.; Wong, M. W.; Andres, J. L.; Gonzalez, C.; Head-Gordon, M.; Replogle, E. S.; Pople, J. A. *Gaussian 98*, Revision A.6; Gaussian, Inc.: Pittsburgh, PA, 1998.
(24) (a) Becke, A. D. *J. Chem. Phys* **1993**, *98*, 1372, 5648. (b) Stephens, P. J.; Devlin, F. J.; Chablowski, C. F.; Frisch, M. J. *J. Phys. Chem.* **1994**, *98*, 11623.
(25) Møller, C.; Plesset, M. S. *Phys. Rev.* **1934**, *46*, 618.
(26) (a) Mayer, I. *Adv. Quantum Chem.* **1980**, *12*, 189. (b) Schlegel, H. B. *J. Chem. Phys.* **1986**, *84*, 4530.
(27) For the various frequency correction factors see, for example: (a) Rauhut, G.; Pulay, R. *J. Phys. Chem.* **1995**, *99*, 3093. (b) Finley, J. W.; Stephens, P. J. *J. Mol. Struct. (THEOCHEM)* **1995**, *227*, 357. (c) Wong, M. W. *Chem. Phys. Lett.* **1996**, *256*, 391. (d) Scott, A. P.; Radom, L. *J. Phys. Chem.* **1996**, *100*, 16502.
(28) (a) Curtiss, L. A.; Raghavachari, K.; Pople, J. A. *J. Chem. Phys.* **1993**, *98*, 1293. (b) Curtiss, L. A.; Raghavachari, K.; Redfern, P. C.; Pople, J. A. *J. Chem. Phys.* **1997**, *106*, 1063. (c) Raghavachari, K.; Stefanov, B. B.; Curtiss, L. A. *J. Chem. Phys.* **1997**, *106*, 6764.
(29) (a) Dunning, T. H., Jr. *J. Chem. Phys.* **1989**, *90*, 1007. (b) Woon, D. E.; Dunning, T. H., Jr. *J. Chem. Phys.* **1993**, *98*, 1358.
(30) (a) Turecek, F. *J. Phys. Chem. A* **1998**, *102*, 4703. (b) Turecek, F.; Wolken, J. K. *J. Phys. Chem. A* **1999**, *103*, 1905. (c) Wolken, J. K.; Turecek, F. *J. Phys. Chem. A*, **1999**, *103*, 6268. (d) Wolken, J. K.; Turecek, F. *J. Am. Chem. Soc.* **1999**, *121*, 6010.
(31) Levine, I. N. *Physical Chemistry*, 3rd ed.; McGraw-Hill: New York, 1988; p 839.
(32) Mallard, W. G., Lindstrom, P. J., Eds. *NIST Chemistry Webbook, NIST Standard Reference Database*; National Institute of Science and Technology: Gaithersburg, MD, 1998; Vol. 69, http://webbook.nist.gov/chemistry.

Table 1. Relative Energies Relevant to the $(CH_3SSCH_3 + H)^+$ System

	relative energy[a]						
species/reaction	B3LYP/ 6-31++G(2d,p)	B3LYP/ 6-311++G(3df,2p)	B3LYP/ aug-cc-pVTZ	MP2/ 6-311++G(3df,2p)	G2 (MP2)	G2++ (MP2)[b]	exp
$CH_3SSCH_3 \rightarrow (CH_3)_2S{-}S$	67	63	67	56	57	57[c] 56[d]	
$CH_3SS(H)CH_3^+ \rightarrow CH_3SSCH_3 + H^+$	804	803	805	789	802	801 806	815
$(CH_3)_2S{-}SH^+ \rightarrow (CH_3)_2S{-}S + H^+$	898	897	899	880	892	891 895	
$CH_3SS(H)CH_3^+ \rightarrow (CH_3)_2S{-}SH^+$	−26	−28	−27	−34	−34	−31 −31	
TS$\{CH_3SS(H)CH_3^+ \rightarrow (CH_3)_2S{-}SH^+\}$		205[c]	203	250	211	214	
$CH_3SS(H)CH_3^+ \rightarrow CH_3SSH^{+\bullet} + CH_3^\bullet$	238	238	235	269		262 267	
$CH_3SS(H)CH_3^+ \rightarrow CH_3SS^+ + CH_4$	117	114	114	123	116	118 121	
$CH_3C{=}NH^+ \rightarrow CH_3CN + H^+$					776 781		779

[a] In units of kJ mol^{-1}. [b] From effective QCISD(T)/6-311++G(3df,2p) energies and scaled B3LYP/6-31++G(2d,p) harmonic frequencies. [c] At 0 K. [d] At 298 K.

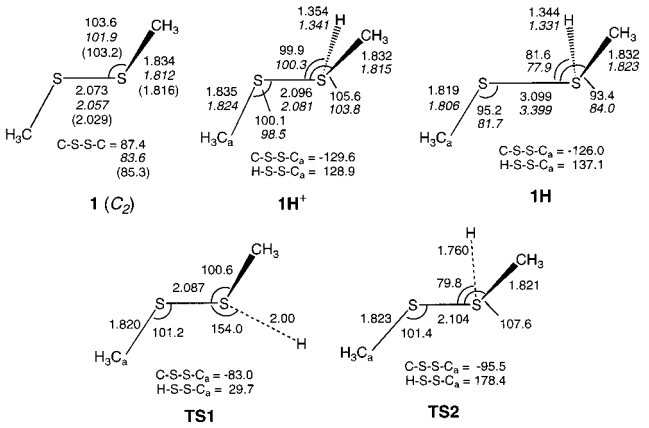

Figure 1. Optimized geometries of **1**, **1H**$^+$, **1H**, and transition states for H atom addition. Bond lengths in angstroms, bond and dihedral angles in degrees. B3LYP/6-31++G(2d,p) geometry parameters are shown by roman types, MP2(FULL)/6-31++G(2d,p) values are shown by italics. Experimental geometry parameters from ref 17b are shown in parentheses.

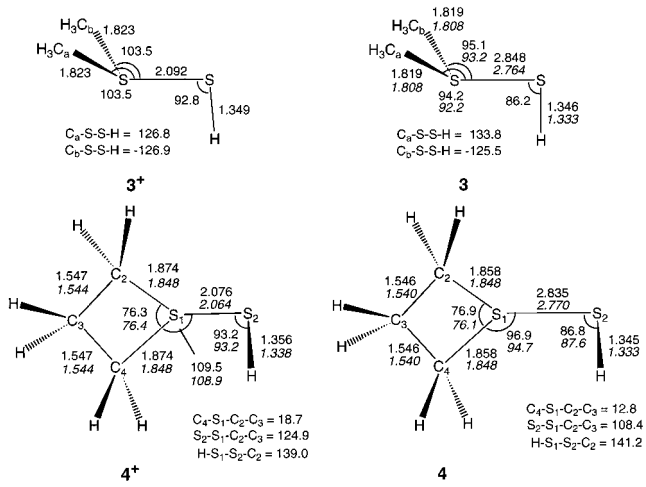

Figure 2. Optimized geometries of **3**$^+$, **3**, **4**$^+$, and **4**. Bond lengths in angstroms, bond and dihedral angles in degrees. B3LYP/6-31++G-(2d,p) geometry parameters are shown by roman types, MP2(FULL)/6-31++G(2d,p) values are shown by italics.

815 kJ mol^{-1}) and acetonitrile (PA = 779 kJ mol^{-1}), reaction 2 was 36 kJ mol^{-1} exothermic, whereas the G2(MP2) calculated proton affinities (Table 1) gave $-\Delta H_r(2) = 26$ and 21 kJ mol^{-1} at 298 and 523 K, respectively. The internal (rotational and vibrational) energy of fully thermalized **1H**$^+$ was calculated as 43 kJ mol^{-1} at 523 K. More exothermic protonations of **1** with H_3O^+ (PA = 691 kJ mol^{-1}, $-\Delta H_{r,298}(2) = 124$ kJ mol^{-1}) and CH_5^+ (PA = 543 kJ mol^{-1}, $-\Delta H_{r,298}(2) = 272$ kJ mol^{-1}) resulted in substantial dissociation of **1H**$^+$ to CH_3SS^+ and methane and thus could not be used to generate precursor ions of intensities sufficient for NR measurements. Interestingly, **1H**$^+$ was less stable than its isomer, *S*-sulfhydryl-*S*,*S*-dimethylsulfonium ion (**3**$^+$, Figure 2). The energy difference for **3**$^+ \rightarrow$ **1H**$^+$ was calculated as 31−34 kJ mol^{-1} at several levels of theory (Table 1). However, **1H**$^+$ and **3**$^+$ were separated by a substantial energy barrier to unimolecular isomerization (211−214 kJ mol^{-1}, Table 1), which should prevent formation of **3**$^+$ from low-energy **1H**$^+$ prepared by the mildly exothermic protonation in eq 1. We show below that the presence of **3**$^+$ was definitely excluded on the basis of the NR mass spectra of **1H**$^+$.

Dissociations of **1H**$^+$ were monitored for metastable ions and following CAD with the goal of identifying small neutral fragments produced from ions. Metastable **1H**$^+$ eliminated CH_4 to form CH_3SS^+; metastable **1D**$^+$ eliminated cleanly CH_3D. CAD of **1H**$^+$ resulted in elimination of H, CH_3, CH_4, (CH_3 + CH_3), (CH_3 + CH_4), H_2S, and CH_3S, as summarized in Table 2. CAD of **1D**$^+$ resulted in elimination of D, CH_3, CH_3D, (CH_3 + CH_3), (CH_3 + CH_3D), HDS, and CH_3S (Table 2), which showed that the sulfonium deuteron did not mix with the hydrogen atoms of the methyl groups. The specific elimination of methane incorporating the sulfonium proton was calculated to require 117 kJ mol^{-1} at the thermochemical threshold at 0 K. The formation of CH_2SSH^+ by loss of methane was less endothermic ($\Delta H_{r,0} = 91$ kJ mol^{-1}) but was not observed in dissociations of metastable **1H**$^+$ or after CAD. This pointed to kinetic control of the methane elimination; the energy barrier for transfer of the sulfonium hydrogen atom is likely to be smaller than that for transfer of the methyl hydrogen atom.

To summarize the ion chemistry part, **1H**$^+$ and **1D**$^+$ were formed unambiguously by mildly exothermic protonation or deuteronation of **1**, respectively. Ion dissociations mostly involved C−S bond cleavages with or without proton transfer.

Hydrogen Atom Adduct to Dimethyl Disulfide. Neutralization of **1H**$^+$ formed transiently the H atom adduct to dimethyl disulfide (**1H**). However, **1H** dissociated completely on the 4.67 μs time scale such that no substantial survivor **1H**$^+$ ion was

Table 2. Collisionally Activated Dissociation Mass Spectra

	relative intensity[a]						relative intensity[a]				
m/z	**1H**$^+$	**1D**$^+$	**2**$^{+\bullet}$	**2H**$^+$	**2D**$^+$	*m/z*	**1H**$^+$	**1D**$^+$	**2**$^{+\bullet}$	**2H**$^+$	**2D**$^+$
15	0.4	0.4				60			2.5	2.1	1.6
26			1.4			61	3.4	5.1	1.8	2.7	1.7
27			2.2	1.5	1.8	62	0.9	0.7			2.1
28		0.3				63		0.5			
32	1.1	1.0	2.3	1.1	1.3	64	10.2	6.5	13.4	6.6	5.6
33	0.5	0.3	1.5			65	1.3	0.4	1.4	2.3	
34		0.4			1.2	66					2.8
35						67	0.6	2.4			
37			1.3		2.5	68					
38			1.7		1.8	69				1.2	1.4
39			4.9	4.0	3.5	70					
40				1.0	1.1	71			1.9	2.1	2.1
41			12.8	7.2	5.1	72			6.0	2.0	
42			1.6	1.3	1.2	73			4.3	20.8	12.1
44	1.7	1.5	1.6	1.3	1.7	74					6.5
45	19.6	13.3	9.4	10.9	10.9	76		0.3			
46	11.3	9.0	3	3.6	4.6	78	0.9	0.9	9.0	2.3	1.6
47	11.1	8.9	2.2	4.9	3.2	79	17.9	15.3		5.2	1.2
47.5	0.9					80	5.9	0.7			4.6
48	4.5	8.2			2.4	81	0.7	9.7			
49	1.3	5.6				83					
50		1.1				93	2.6	0.4			
51						94	5.4	6.0			
52		0.4				95		0.7			
53.5				2.7		105			1.8		
54					2.9	106				5.6	3.3
57			1.6	1.2	1.1	107					1.5
58			3.8	3.1	2.6						
59			6.7	3.2	3.0						

[a] Relative to the sum of product ion intensities, $\%\sum I_{CAD}$.

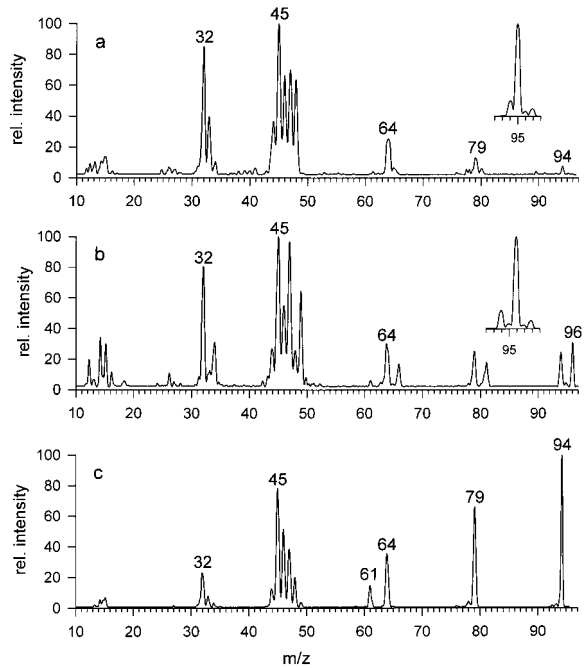

Figure 3. Neutralization (CH_3SSCH_3, 70% transmittance)−reionization (O_2, 70% transmittance) mass spectra of (a) **1H**$^+$, (b) **1D**$^+$, and (c) **1**$^{+\bullet}$. Insets show the $(M + H,D)^+$ regions in the chemical ionization mass spectra.

found in the NR spectrum (Figure 3a). Note that formation of **1H**$^+$ by protonation of **1** contained 0.5% of combined ^{13}C and ^{33}S isotopomers of **1**$^{+\bullet}$ (Figure 3a, inset), which were not resolved from isobaric **1H**$^+$ and may have contributed to the very weak residual peak at *m/z* 95 (Figure 3a). The major NR dissociations of **1H** were loss of H$^\bullet$ to form **1** (*m/z* 94), loss of $CH_3^\bullet$ to form CH_3SSH (*m/z* 80), elimination of CH_4 to form $CH_3SS^\bullet$ (*m/z* 79), and loss of $CH_3S^\bullet$ to form CH_3SH (*m/z* 48). Secondary dissociations formed $SSH^\bullet$ (*m/z* 65), S_2 (*m/z* 64), $CH_{1-3}S$ (*m/z* 45−47), and $SH^\bullet$ (*m/z* 33). Stable neutral products were characterized by their reference NR mass spectra (not shown), which showed prominent survivor ions for **1**, S_2, CH_3SCH_3,[11,16h] CH_3SS, CH_3SH,[11] and CH_2SH. Note that the peak of ionized CH_3SCH_3 (*m/z* 62) was practically absent in the NR mass spectrum of **1H**$^+$. Since CH_3SCH_3 was the expected product of dissociation of the isomeric radical **3** (vide infra), its absence in the NR spectrum provided strong evidence that **3**$^+$ was not present in the precursor ion beam.

NR of **1D**$^+$ showed a survivor ion at *m/z* 96 (Figure 3b). However, **1D**$^+$ was contaminated by 1.7% of an isobaric ^{34}S isotopomer of **1**$^{+\bullet}$ (Figure 3b, inset), which could partially account for the peak at *m/z* 96. Dissociations of **1D** showed clean loss of D (*m/z* 94), eliminations of CH_3 (*m/z* 81), CH_3D (*m/z* 79), CH_3S (*m/z* 49), and formations of SSD (*m/z* 66), S_2 (*m/z* 64), and SD (*m/z* 34). Hence, the spectra clearly showed that *not only the S−S bond but also the S−H and S−C bonds were cleaved* in the hypervalent radical **1H** following vertical electron capture by the **1H**$^+$ ion.

To interpret the radical dissociations we used the structures (Figure 1) and energies calculated for the **1H** system (Table 3). **1H** was found as a local energy minimum at several levels of theory, as confirmed by frequency analysis. However, electron capture in **1H**$^+$ → **1H** resulted in substantial geometry changes (Figure 1). In particular, the S−S bond in **1H** was 48% longer than that in **1H**$^+$, and the bond angles about the tricoordinated sulfur atom indicated inward rotation of the methanethiol moiety (Figure 1). Consequently, the dissociation energy of the long S−S bond in **1H** was only 8 kJ mol^{-1} at 0 K by G2++(MP2). Vertical electron capture in **1H**$^+$ was accompanied by large Franck−Condon effects and formed **1H** with 160−230 kJ mol^{-1} internal energy (Table 3). This excitation in **1H** was more than sufficient to break the weak S−S bond. Moreover, the internal energy was sufficient to break the S−H and C−S bonds that had G2++(MP2) dissociation energies of 96 and 52 kJ mol^{-1}, respectively, at 0 K (Table 3).

The isomeric *S*-sulfhydryl-*S*,*S*-dimethylsulfonium radical **3** (Figure 2) was calculated to be 15 kJ mol^{-1} more stable than **1H**, which paralleled the relative stabilities of ions **1H**$^+$ and **3**$^+$. Radical **3** was bound by only 26 kJ mol^{-1} against dissociation to $(CH_3)_2S$ and $SH^\bullet$, which could be supplied by the large Franck−Condon energy upon vertical neutralization of **3**$^+$, E_{FC} = 120−140 kJ mol^{-1}. The absence of $(CH_3)_2S$ in the NR spectrum indicated that **3** was *not* formed by isomerization of **1H** nor by ion isomerization **1H**$^+$ → **3H**$^+$ followed by neutralization of the latter ion.

Reaction Paths for 1 + H$^\bullet$ Addition. The formation of the S−H bond in **1H** by hydrogen atom capture by **1** was substantially exothermic, $\Delta H_{r,0} = -96$ kJ mol^{-1} (Table 3). Hence, if the energy released by the exothermic addition of a hydrogen atom to **1** was stored in vibrationally excited **1H**, it would be sufficient to drive dissociation of both the S−S and S−C bonds adjacent to the hypervalent sulfur atom, but not the other sulfidic S−C bond (Table 3). The H atom addition was investigated in detail by B3LYP and MP2 calculations that revealed two reaction paths. A rear attack by a H atom at the sulfur atom along the S−S bond in dimethyl disulfide proceeded through a first-order saddle point in the transition state (**TS1**) that was located by MP2 calculations (Figure 4). In contrast, the B3LYP potential energy profile was continuously decreasing along the reaction path and indicated no barrier for the addition. Single-point G2++(MP2) calculations along the MP2 reaction path confirmed the existence of a barrier which was 9 kJ mol^{-1}

Table 3. Relative Energies Relevant to the $(CH_3SSCH_3 + H)^{\bullet}$ System

	relative energy[a]						
species/reaction	B3LYP/ 6-31++G(2d,p)	B3LYP/ 6-311++G(3df,2p)	B3LYP/ aug-cc-pVTZ	PMP2/ 6-311++G(3df,2p)	G2 (PMP2)	G2++ (PMP2)[b]	exp
$CH_3SSCH_3 \rightarrow 2CH_3S^{\bullet}$	228	233	227	263	272	275[c]	
						277[d]	270 ± 6[e]
$CH_3SSCH_3 \rightarrow CH_3SS^{\bullet} + CH_3^{\bullet}$	209	209		243	247	236	
						240	251 ± 7[f]
$CH_3SS(H)CH_3^{\bullet} \rightarrow CH_3SSCH_3 + H^{\bullet}$	123	120	123	83		96	
						98	
$CH_3SS(H)CH_3^{\bullet}$ (VN)		161	169	230			
$CH_3SS(H)CH_3^{\bullet} \rightarrow CH_3SS(H)CH_3^{+}$	635	632	637	605		608	
	(6.58)[g]	(6.55)	(6.60)	(6.28)		(6.30)	
$CH_3SS(H)CH_3^{+} \rightarrow CH_3SS(H)CH_3^{\bullet}$		−463[h]	−459	−367			
$CH_3SS(H)CH_3^{\bullet}$ (VN) $\rightarrow CH_3SSCH_3 + H^{\bullet}$		−41	−46	−147			
$CH_3SSCH_3 + H^{\bullet} \rightarrow$ **TS1**						9	
$CH_3SSCH_3 + H^{\bullet} \rightarrow$ **TS2**						33	
$CH_3SS(H)CH_3^{\bullet} \rightarrow CH_3S^{\bullet} + CH_3SH$	5.5	4.7	3.6	7.5		8.0	
						6.1	
$CH_3SS(H)CH_3^{\bullet} \rightarrow CH_3S-SH + CH_3^{\bullet}$	53	50	51	52		52	
						54	
$CH_3S(H)SCH_3^{\bullet} \rightarrow CH_3S(H)\text{-}S + CH_3^{\bullet}$	145	138	144	141		140	
						140	
$CH_3SS(H)CH_3^{\bullet} \rightarrow (CH_3)_2S-SH^{\bullet}$	−14	−15	−14	−16		−15	
						−16	
$(CH_3)_2S-SH^{\bullet} \rightarrow (CH_3)_2S-S + H^{\bullet}$		197	204	155		169	
						170	
$(CH_3)_2S-SH^{\bullet} \rightarrow (CH_3)_2S + SH^{\bullet}$		30		26		26	
						27	
$(CH_3)_2S-SH^{\bullet}$ (VN) $\rightarrow (CH_3)_2S + SH^{\bullet}$		−110		−94			
$(CH_3)_2S-SH^{\bullet} \rightarrow CH_3S-SH + CH_3^{\bullet}$		64	65	70		68	
						70	

[a] In units of kJ mol^{-1}. [b] From effective QCISD(T)/6-311++G(3df,2p) energies and scaled B3LYP/6-31+G(2d,p) harmonic frequencies. [c] At 0 K. [d] At 298 K. [e] Reference 41. [f] Reference 43. [g] Adiabatic ionization energies (electronvolts). [h] Vertical recombination energies.

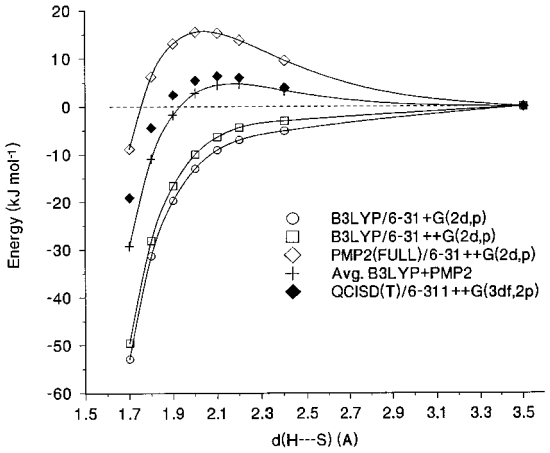

Figure 4. Potential energy profiles for H atom additions to **1** through **TS1**.

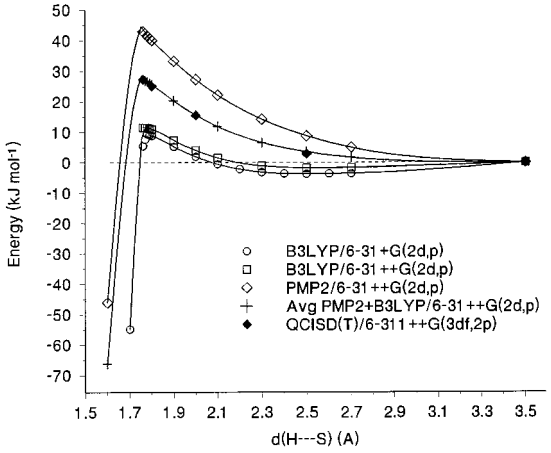

Figure 5. Potential energy profiles for H atom additions to **1** through **TS2**.

above the reactants. It was previously found for several systems that MP2 barriers for H atom addition were typically overestimated while the B3LYP barriers were underestimated,[30b−d] which also appeared to be the case for **1**. However, averaging the PMP2 and B3LYP energies resulted in a very good fit with the G2++(MP2) energies; the PMP2/B3LYP averaged transition state was 7 kJ mol^{-1} above the reactants (Figure 4).

A different reaction path resulted from a hydrogen atom attack at the sulfur atom perpendicular to the S−S bond (Figure 5). In this case, both PMP2 and B3LYP showed transition states (**TS2**, Figure 1) that differed in the heights of the potential energy barriers (Figure 5). G2++(MP2) single-point calculations gave the **TS2** energy as 33 kJ mol^{-1} above the reactants. This was approximated reasonably well by averaged PMP2/B3LYP calculations that gave the **TS2** energy as 22 kJ mol^{-1} above the reactants (Figure 5).

Hydrogen Atom Addition Kinetics. The energy barriers for H atom additions to dimethyl disulfide were used to calculate thermal rate constants at the high-pressure limit. Hydrogen atom tunneling was neglected. At 298 K, addition through **TS1** was 10^4-fold faster than addition through **TS2**, and the differences remained substantial even at higher temperatures (Figure 6). Hence, the hydrogen atom addition was under strict stereoelectronic control[33,34] that preferred the rear attack. When applied to electron capture dissociation (ECD) of partially neutralized peptide ions,[7,8] the disulfide bond cleavage by hydrogen atom capture should depend on the mutual orientation of the hydrogen

(33) For a comprehensive review, see: (a) Deslongchamps, P. *Stereoelectronic Effects in Organic Chemistry*; Pergamon: Oxford, 1983.

(34) For a discussion of stereoelectronic effects in gas-phase ion reactions, see: (a) Turecek, F.; Hanus, V. *Advances in Mass Spectrometry, 1985*; Todd, J. F. J., Ed.; Wiley: New York, 1986; pp 215−224. (b) Turecek, F. *Int. J. Mass Spectrom. Ion Processes* **1991**, *108*, 137.

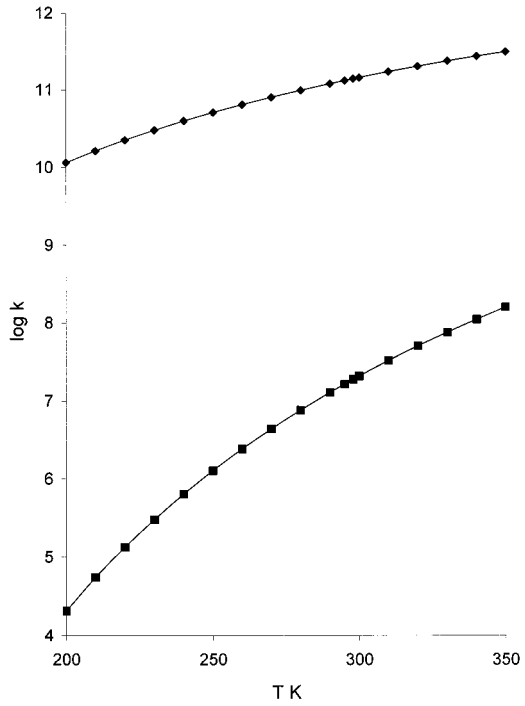

Figure 6. Thermal rate constants for H atom addition to **1** at the high-pressure limit. (◆) Addition through **TS1**; (■) addition through **TS2**.

atom donor and the disulfide bond. A hydrogen atom departing a donor, e.g., a vibrationally excited C•(OH)NH group,[8] should preferentially attack a disulfide bond that is oriented along the approach trajectory. Disulfide bonds perpendicular to the approach trajectory would face higher energy barriers to the hydrogen capture. The stereochemical selectivity due to the disulfide bond orientation is likely to decrease in capture of hot hydrogen atoms whose kinetic energies exceed substantially the potential energy barrier for the addition. This theory could be tested by ECD of a multiply charged and conformationally restricted peptide ion in which the stereochemistry of the protonation sites and two different disulfide bonds is well known and cleavage of the disulfide bonds results in distinguishable fragment ions. Conversely, the stereochemistry of disulfide bond cleavage on ECD may be useful for determining the peptide ion three-dimensional structure.

Protonation of 1,2-Dithiolan. Precursor cations for the cyclic disulfide adducts **2H** and **2D** were generated by gas-phase protonation or deuteronation of **2**. According to the calculated proton affinity of **2** (823 kJ mol^{-1} by averaged MP2 and B3LYP calculations, Table 4), **2** can be protonated exothermically with *t*-$C_4H_9^+/C_4H_{10}$ (PA = 801 kJ mol^{-1}), $CH_3OH_2^+/CH_3OH$ (PA = 754 kJ mol^{-1}),[32] or $CH_3C{=}NH^+/CH_3CN$, all of which were used for the efficient formation of $\mathbf{2H}^+$. Ion $\mathbf{2D}^+$ was prepared by deuteronation with $CD_3OD_2^+/CD_3OD$ and $CD_3C{=}ND^+/CD_3CN$. Ions $\mathbf{2H}^+$ and $\mathbf{2D}^+$ were characterized by CAD spectra (Table 2) that revealed the dissociation products, and by combined B3LYP/MP2 calculations that provided the dissociation energies. Loss of H_2S was calculated to be the lowest-energy dissociation of $\mathbf{2H}^+$ (Table 4) and dominated the metastable ion spectra. The S-bound proton underwent exchange with the other ring hydrogens, such that metastable $\mathbf{2D}^+$ eliminated HDS and H_2S in a ≈1:1 ratio (Table 2). The detailed mechanism of the H_2S elimination was beyond the scope of this work and was not studied. Collisional activation of $\mathbf{2H}^+$ resulted in losses of H, C_2H_4, C_2H_5, and H_2S. Complementary $S_2^{+\bullet}$ and S_2H^+ ions were also observed. CAD of $\mathbf{2D}^+$ showed loss of D and H in a 2.2:1 ratio, a clean elimination of C_2H_4, and loss of HDS and H_2S in a 2:1 ratio. Interestingly, $\mathbf{2H}^+$ was calculated to be 39 kJ mol^{-1} more stable than isomeric 1-sulfhydrylthietanium cation $\mathbf{4}^+$ (Figure 2, Table 4). This stability reversal, compared with $\mathbf{1H}^+/\mathbf{3}^+$, was probably due to an increased strain in the four-membered ring of $\mathbf{4}^+$. Ring opening in $\mathbf{2H}^+$ by S—S bond cleavage provided an unstable $HSCH_2CH_2CH_2S^+$ cation that rearranged spontaneously to $HSCH_2CH_2CH{=}SH^+$; the latter was 63 kJ mol^{-1} less stable than $\mathbf{2H}^+$ (Table 4). The instability of singlet alkylthiyl cations has been noted previously for CH_3S^+.[35] Ring dissociations yielding CH_2SSH^+ (*m*/*z* 79) and SSH^+ (*m*/*z* 65) that were observed upon CAD (Table 2) were both substantially endothermic (Table 4).

Hydrogen Atom Adducts to 1,2-Dithiolan. Neutralization of $\mathbf{2H}^+$ formed the H atom adduct **2H**. In contrast to **1H**, NR of $\mathbf{2H}^+$ did not result in complete dissociation, and a moderately abundant survivor ion was observed at *m*/*z* 107 (Figure 7a). Loss of H (*m*/*z* 106) was a major dissociation of **2H** upon NR. Deuterium labeling in $\mathbf{2D}^+$ revealed loss of D and H in a 5:1 ratio (Figure 7b). Hence, the loss of D from the hypervalent sulfur atom in **2D** was predominant but not exclusive. Further dissociations of **2** formed from **2H** or **2D** were distinguished on the basis of a reference NR spectrum of $\mathbf{2}^{+\bullet}$ (Figure 7c), which was qualitatively similar to the standard electron ionization mass spectrum.[22] Fragments that distinguished NR dissociations of **2H** and $\mathbf{2}^{+\bullet}$ were identified from the mass shifts due to the presence of the S-deuterium in **2D**. The dissociation products of **2H** included SSH^+ (*m*/*z* 65) that shifted to SSD^+ (*m*/*z* 66), $C_3H_5^+$ (*m*/*z* 41) that shifted in part to $C_3H_4D^+$ (*m*/*z* 42), and HS^+ (*m*/*z* 33) that shifted to DS^+ (*m*/*z* 34). A new dissociation product of **2H** that was not present in the CAD spectrum of $\mathbf{2H}^+$ was observed at *m*/*z* 74 due to elimination of HS (DS from **2D**). Also noteworthy was the isotope effect on the loss of D from **2D**, which was apparent from the diminished formation of **2** (*m*/*z* 106) and its signature NR dissociation products (*m*/*z* 78, 41, Figure 7b,c). The NR spectra of **2H** and **2D** pointed to a specific cleavage of the S—(H,D) bond and a ring opening by cleavage of the S—S or S—C bonds. The products of the latter two dissociations were isomeric radicals that were not distinguished experimentally.

A further insight into the chemistry of **2H** was obtained from ab initio and density functional calculations (Table 4). **2H** was found to be a bound structure (Figure 8). The S—S bond in **2H** was substantially longer than those in **2** and $\mathbf{2H}^+$ (Figure 8). Consequently, ring opening in **2H** by cleavage of the long S—S bond to form $HSCH_2CH_2CH_2S^\bullet$ (*syn*- and *anti*-**5**, Figure 9) required only 10−11 kJ mol^{-1} (Table 4). Other dissociations of **2H** were more endothermic. Cleavage of the C—S bond to form $HSSCH_2CH_2CH_2^\bullet$ (*syn*- and *anti*-**6**, Figure 9) required 43 kJ mol^{-1}, whereas dissociation of the S—H bond to form **2** and H• required 118 kJ mol^{-1} (Scheme 3). Isomerization to 1-sulfhydrylthietanium radical **4** (Figure 8) was 59 kJ mol^{-1} endothermic (Table 4). Note that the S—S, C—S, and S—H bond cleavages in **2H** and isomerization to **4** could be driven by the Franck−Condon energy acquired by vertical neutralization of $\mathbf{2H}^+$, which was calculated to be 142 kJ mol^{-1} (Table 4).

The open-ring radical intermediates *syn*- and *anti*-**5** and -**6** can undergo several dissociations, which were investigated computationally (Scheme 3). In order of increasing endothermicities, formations of SSH• and cyclopropane, SH• and thietane, $CH_2SSH^\bullet$ and ethylene, $HSCH_2CH_2^\bullet$ and $CH_2{=}S$, and $HSCH_2CH_2CH{=}S$ and H• required $\Delta H_{r,0}$ = 38, 85, 110, 156, and 188

(35) Sumathi, R.; Peyerimhoff, S. D.; Sengupta, D. *J. Phys. Chem. A* **1999**, *103*, 772.

Table 4. Relative Energies Relevant to the (1,2-Dithiolan + H) System

species/reaction	relative energy[a] B3LYP/6-31++G(2d,p)	B3LYP/6-311++G(2df,p)	PMP2/6-311++G(2df,p)	avg[b]
2H$^+$ → **2** + H$^+$	829	827	809	817[c] 823[d]
2H$^+$ → **4**$^+$	36	35	43	39 41
2H$^+$ → HS−CH_2CH_2CH=SH^+	57	58	69	63 66
2H$^+$ → H_2S + CH_2=CH−CH=SH^+	75	72	135	103 111
2H$^+$ → CH_2=SSH^+ + C_2H_4	175	164	223	194 201
2H$^+$ → SSH^+ + cyc-C_3H_6	314	304	337	321 325
2H → **2H**$^+$ (IE_a)[e]	633 (6.56)[e]	632 (6.55)	596 (6.18)	614 (6.36)
2H$^+$ → **2H** (VN)[f]		−472	−458	−465
2H → **2** + H$^\bullet$	144	140	95	118 121
2H (VN) → **2** + H$^\bullet$		−13	−36	−25
2H → **4**	55	54	63	59 61
2H → *anti*-**5**	4	12	7	10 11
2H → *syn*-**5**	15	14	9	11 12
2H → *anti*-**6**	43	40	46	43 47
2H → *syn*-**6**	44	40	45	43 46
2H → $SSH^\bullet$ + cyc-C_3H_6	33	25	52	38 40
TS4 (*anti*-**6** → $SSH^\bullet$ + cyc-C_3H_6)	52	96	101	99
2H → **TS4**		136	164	150
2H → thietane + $SH^\bullet$	85	84	85	85 88
2H → **7**	59	59	69	64 66
anti−**6** → *anti*-**8**	−132	−132	−133	−132 −135
TS5 (*syn*-**6** → **7**)	68	70	68	69
2H → **TS5**		82	86	84
2H → $CH_2SSH^\bullet$ + C_2H_4	99	88	132	110 116
2H → HS−$CH_2CH_2\bullet$ + CH_2=S	145	141	169	156 162
2H → HS−CH_2CH_2CH=S+ H$^\bullet$	204	201	174	188 194

[a] In units of kJ mol^{-1}. [b] From averaged PMP2 and B3LYP/6-311++G(2df,p) energies. [c] At 0 K. [d] At 298 K. [e] Adiabatic ionization energies (electronvolts). [f] Vertical recombination energies.

kJ mol^{-1} from **2H**, respectively (Table 4). The lowest-energy dissociation of *anti*-**6** to $SSH^\bullet$ and cyc-C_3H_6 was calculated to be 5 kJ mol^{-1} exothermic (Table 4). The existence of bound structures *syn*- and *anti*-**6** was due to an energy barrier for the intramolecular radical substitution forming the cyclopropane ring through **TS4**, E_a = 99 kJ mol^{-1} above *anti*-**6** (Scheme 3). In contrast, intramolecular attack by the terminal methylene radical at the inner sulfur atom in *syn*-**6** was endothermic and showed no activation barrier above the dissociation threshold for the formation of separated thietane and $SH^\bullet$. The dissociation was found to proceed through a low-lying transition state (**TS5**, 69 kJ mol^{-1} above *syn*-**6**) to form a van der Waals complex of thietane and $SH^\bullet$ (**7**) that was bound by 21 kJ mol^{-1} against dissociation.[36] Another isomer, *anti*-$CH_3CH_2CH_2SS^\bullet$ (*anti*-**8**), was identified by calculations that was substantially more stable than **2H**-**6** (Table 4). The stability of *anti*-**8** compared with *anti*-**6** ($\Delta H_{r,298}$(**6** → **8**) = −135 kJ mol^{-1}) reflects the difference in the C−H and S−H bond dissociation energies. Interestingly, exothermic isomerization of **6** to **8** was not observed to accompany dissociations of **2H**. This was judged from the absence of a $C_3H_7^+$ ion in the NR mass spectrum (Figure 7a), which would be an expected fragment from dissociations of reionized **8**. The absence of exothermic isomerization **6** → **8** is probably due to its unfavorable kinetics.

Cations corresponding to reionized dissociation products, $HSCH_2CH_2CH{=}S^{+\bullet}$, thietane$^{+\bullet}$, CH_2SSH^+, $C_3H_6^{+\bullet}$, SSH^+, $CH_2S^{+\bullet}$, and HS^+, were present in the NR mass spectrum of **2H** (Figure 7a) but mostly overlapped with the dissociation products of reionized **2**$^{+\bullet}$ (Figure 7c). The non-decomposing radicals that were detected by NR were probably due to a fraction of low-energy **2H** at equilibrium with **5** and **6**. For **2H** having vibrational energies below the lowest dissociation threshold to $SH^\bullet$ and thietane (Table 4), the calculated ΔG for **2H** → *anti*-**5**, *syn*-**5**, *anti*-**6**, and *syn*-**6**, (−0.8, 3.6, 16.9, and 20.8 kJ mol^{-1}, respectively) indicated a 35:39:21:3:2 mixture of **2H**, *anti*-**5**, *syn*-**5**, *anti*-**6**, and *syn*-**6**.[37] Despite the large Franck−Condon effects in vertical neutralization of vibrationally relaxed **2H**$^+$, a fraction of low-energy **2H** can arise from

(36) Uncorrected for basis set superposition error.

(37) The maximum vibrational energy in nondissociating **2H** (85 kJ mol^{-1}) was converted to an effective temperature (875 K) that was used to calculate the ΔH_{875}, ΔS_{875}, and ΔG_{875} for the equilibrium of **2H**, *anti*-5, *syn*-**5**, *anti*-**6**, and *syn*-**6**.

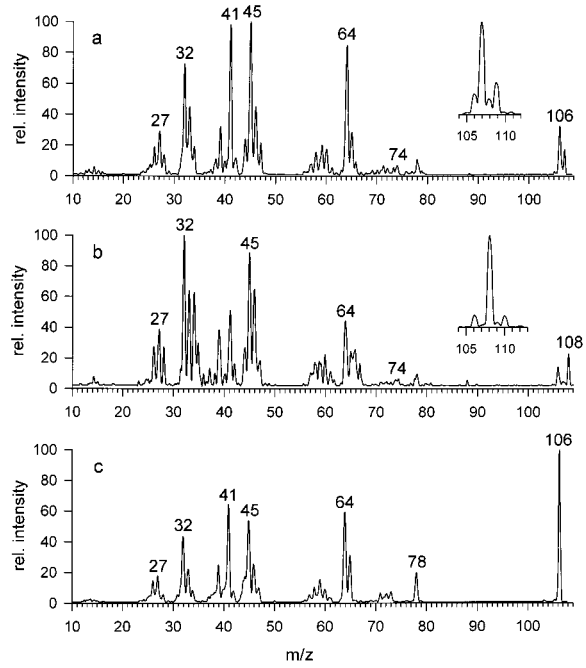

Figure 7. Neutralization (CH_3SSCH_3, 70% transmittance)−reionization (O_2, 70% transmittance) mass spectra of (a) $\mathbf{2H}^+$, (b) $\mathbf{2D}^+$, and (c) $\mathbf{2}^{+\bullet}$. Insets show the $(M + H,D)^+$ regions in the chemical ionization mass spectra.

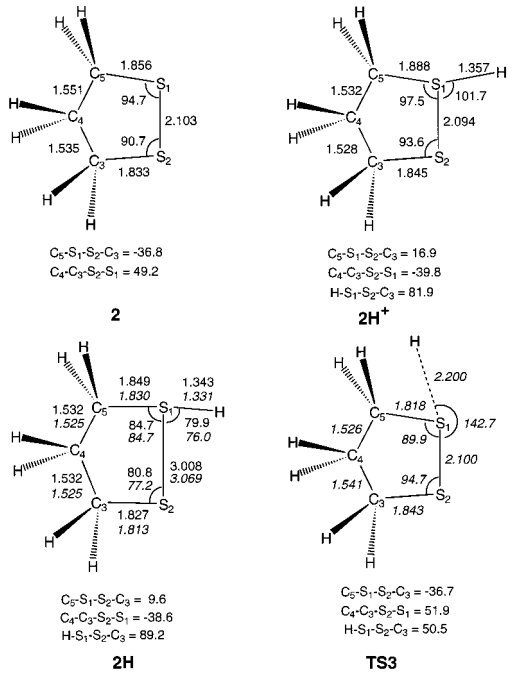

Figure 8. Optimized geometries of **2**, $\mathbf{2H}^+$, **2H**, and **TS3**. Bond lengths in angstroms, bond and dihedral angles in degrees. B3LYP/6-31++G(2d,p) geometry parameters are shown by roman types, MP2(FULL)/6-31++G(2d,p) values are shown by italics.

vibrationally excited cations.[38] For **2H** formed by vertical electron transfer, the Franck−Condon energy was mostly due to the mismatch of the S−S bond lengths in the ion and radical (Figure 8). The vibrational modes that included S−S bond stretch in $\mathbf{2H}^+$ were soft, ν = 375, 443, and 479 cm^{-1}, so that a 30−40% fraction of $\mathbf{2H}^+$ formed by exothermic protonation

(38) (a) Nguyen, V. Q.; Shaffer, S. A.; Turecek, F.; Hop, C. E. C. A. *J. Phys. Chem.* **1995**, *99*, 15454. (b) Frank, A. J.; Turecek, F. *J. Phys. Chem. A* **1999**, *103*, 5348. (c) Polasek, M.; Turecek, F. *J. Phys. Chem. A* **1999**, *103*, 9241.

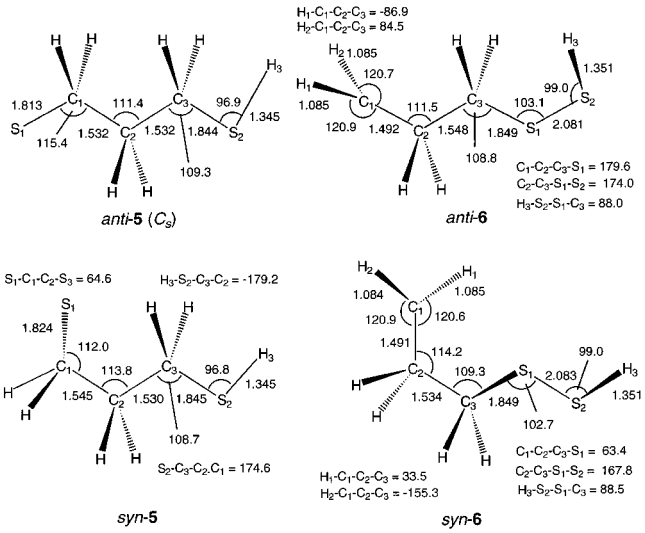

Figure 9. B3LYP/6-31++G(2d,p) optimized geometries of *syn*- and *anti*-**5** and -**6**. Bond lengths in angstroms, bond and dihedral angles in degrees.

Scheme 3

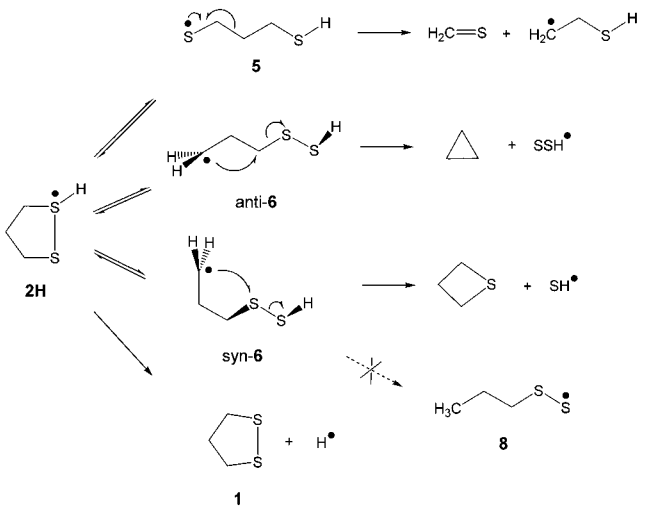

at 523 K existed in $\upsilon \geq 1$ vibrational states.[39] Vertical neutralization of excited vibrational states of $\mathbf{2H}^+$ yielded fractions of **2H** in which the S−S bond was stretched, which resulted in a closer match with the relaxed geometry of the radical. Hence, a fraction of **2H** could be formed with internal energies close to or below the lowest dissociation threshold forming thietane and SH$^\bullet$ ($\Delta H_{diss,0}$ = 85 kJ mol^{-1}, Table 4). Some of the metastability of neutralized **2H** can also be due to the kinetic shift[40] in the dissociations occurring on the microsecond time scale.

Reaction Path for 2 + H$^\bullet$ Addition. The reaction path for hydrogen atom addition to **2** was investigated by B3LYP and

(39) Calculated according to the published method: Dunbar, R. C. *J. Chem. Phys.* **1989**, *90*, 7369.

(40) Lifshitz, C. *Mass Spectrom. Rev.* **1982**, *1*, 309.

(41) From the heats of formation of CH_3SSCH_3 (−24.1 ± 2.3 kJ mol^{-1}, ref 32) and $CH_3S^\bullet$ (139 ± 6 kJ mol^{-1}, ref 42).

(42) McMillen, D. F.; Golden, D. M. *Annu. Rev. Phys. Chem.* **1982**, *33*, 493.

(43) From the heats of formation of $CH_3^\bullet$ (145.7 kJ mol^{-1}, ref 44; 147.1 ± 1 kJ mol^{-1}, ref 45) and $CH_3SS^\bullet$ (80.2 ± 6 kJ mol^{-1}). The latter value was based on an appearance energy measurement (ref 46), the revised $\Delta H_{f,298}(t\text{-}C_4H_9^+)$ = 710.9 ± 3.8 kJ mol^{-1} (ref 32), and corrected for the product enthalpies at 298 K (+27 kJ mol^{-1}, ref 47).

(44) Chase, M. W., Jr. *NIST-JANAF Themochemical Tables*, 4th ed.; Journal of Physical and Chemical Reference Data, Monograph 9; American Institute of Physics: Woodbury, NY, 1998; pp 1−1951.

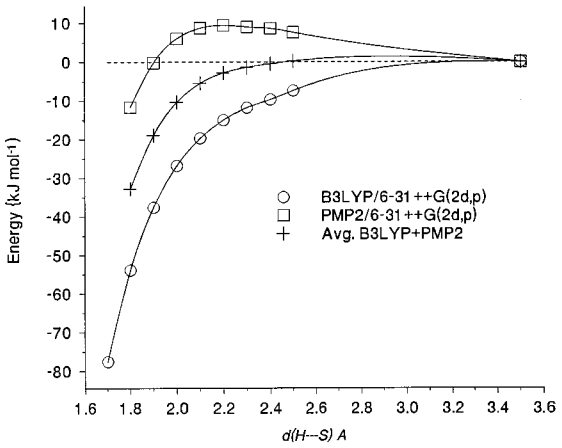

Figure 10. B3LYP and PMP2/6-31++G(2d,p) potential energy profiles for H atom additions to **2**.

MP2 calculations with the 6-31++G(2d,p) basis set (Figure 10). Similar to **1H**, an exothermic addition of H to **2** ($\Delta H_{r,0} = -118$ kJ mol^{-1}) would provide **2H** with sufficient energy to break the S—S and S—C bonds adjacent to the hypervalent sulfur atom. The B3LYP potential energy surface along the H—S coordinate was continuously decreasing and indicated no barrier for the addition. In contrast, the PMP2 potential energy surface (Figure 10) showed a small barrier at d(H—S) = 2.2 Å in a transition state (**TS3**, Figure 8). Since the PMP2 calculations typically overestimate the barriers for H additions while B3LYP calculations underestimate them (cf. Figure 4),[30b−d] a more realistic description was provided by the averaged energies which showed no barrier. Interestingly, both the B3LYP and MP2 calculations showed only a single pathway for the H atom addition. In the MP2 transition state, the H atom approached the sulfur atom at a large angle to the S—S bond (Figure 8). The addition essentially proceeded by a rear attack at the sulfur atom, analogous to **TS1** for a H atom addition to dimethyl disulfide. The absence of an energy barrier to H atom addition can be attributed to a release of Coulomb repulsion between nonbonding electrons in the eclipsed p-orbitals on the vicinal sulfur atoms in **2**. The latter carry negative atomic charges, as shown in Scheme 4. Upon approach of the hydrogen atom, the electron density flows to the departing sulfur atom and, in part, into the forming S—H bond, as documented by the calculated atomic charges and spin densities of the reactants, **TS3**, and product **2H** (Scheme 4, spin densities in parentheses). The addition of H can be viewed as proceeding through an early transition state, which is consistent with the fact that the addition is substantially exothermic (Table 4).

Scheme 4

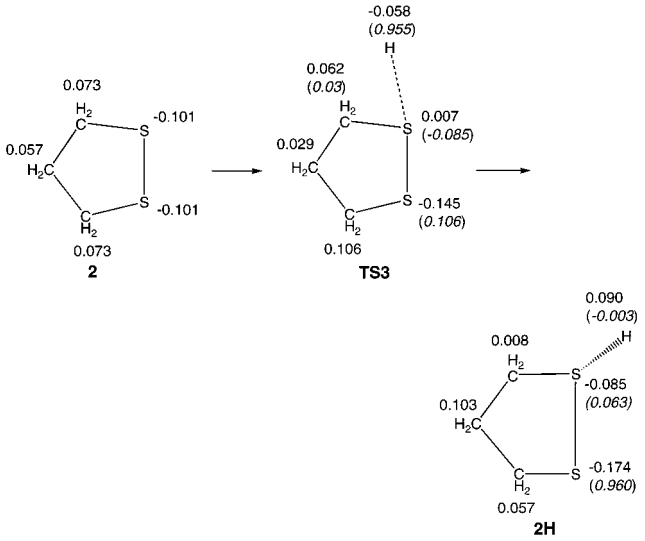

Conclusions

When generated by collisional neutralization of stable cations **1H**$^+$ and **2H**$^+$, radicals **1H** and **2H** dissociated by cleavages of H—S, C—S, and S—S bonds adjacent to the hypervalent sulfur atom. This differed from the S—S bond dissociation selectivity induced by electron capture in multiply charged peptide ions.[7,8] Hydrogen atom capture by the disulfide bond was calculated to be substantially exothermic regardless of the disulfide bond conformation. However, H atom addition to the staggered disulfide bond in dimethyl disulfide showed two distinct reaction paths that differed in the transition state energies. Rear attack by the hydrogen atom was kinetically preferred in dimethyl disulfide, and it was the only reaction path found for H addition to the eclipsed disulfide bond in 1,2-dithiolan. Stereoelectronic effects are predicted for intramolecular hydrogen atom capture in neutralized peptides containing disulfide bonds.

Acknowledgment. Support of this work by NSF (Grant CHE-9712750) is gratefully acknowledged. Computational support was provided by the Department of Chemistry Computer Facility which received generous funding from NSF (Grant CH-9808182) and University of Washington.

Supporting Information Available: Tables of total energies, optimized geometries, and harmonic frequencies (PDF). This material is available free of charge via the Internet at http://pubs.acs.org.

JA993789Q

(45) Tsang, W. In *Energetics of Organic Free Radicals*; Martinho Simoes, J. A., Greenberg, A., Liebman, J. F., Eds.; Blackie Academic and Professional: London, 1996; pp 22−58.

(46) Hawari, J. A.; Griller, D.; Lossing, F. P. *J. Am. Chem. Soc.* **1986**, *108*, 3273.

(47) Traeger, J. C.; McLoughlin, R. G. *J. Am. Chem. Soc.* **1981**, *103*, 3647.